ISSN 0021-3640, JETP Letters, 2018, Vol. 108, No. 1, pp. 71–83. © Pleiades Publishing, Inc., 2018.

SCIENTIFIC SUMMARIES

Noise Insights into Electronic Transport[1]

S. U. Piatrusha[a, b], L. V. Ginzburg[a, b], E. S. Tikhonov[a, b], D. V. Shovkun[a, b], G. Koblmüller[c], A. V. Bubis[a, b, d], A. K. Grebenko[b, d], A. G. Nasibulin[d, e], and V. S. Khrapai[a, f, *]

[a] *Institute of Solid State Physics, Russian Academy of Sciences, Chernogolovka, Moscow region, 142432 Russia*

[b] *Moscow Institute of Physics and Technology (State University), Dolgoprudnyi, Moscow region, 141700 Russia*

[c] *Walter Schottky Institut, Physik Department, and Center for Nanotechnology and Nanomaterials, Technische Universität München, Garching, 85748 Germany*

[d] *Skolkovo Institute of Science and Technology, Moscow, Russia*

[e] *Department of Applied Physics, School of Science, Aalto University, Aalto, FI-00076 Finland*

[f] *Department of Physics, Moscow State University of Education, Moscow, 119435 Russia*

**e-mail: dick@issp.ac.ru*

Received May 8, 2018; in final form, June 5, 2018

Typical experimental measurement is set up as a study of the system's response to a stationary external excitation. This approach considers any random fluctuation of the signal as spurious contribution, which is to be eliminated via time-averaging, or, equivalently, bandwidth reduction. Beyond that lies a conceptually different paradigm—the measurement of the system's spontaneous fluctuations. The goal of this overview article is to demonstrate how current noise measurements bring insight into hidden features of electronic transport in various mesoscopic conductors, ranging from 2D topological insulators to individual carbon nanotubes.

DOI: 10.1134/S0021364018130039

1. INTRODUCTION

Back in 1918, in his research for factors limiting the performance of hot cathode amplifiers, Walter Schottky was the first to understand that discreteness of the elementary charge, e, gives rise to current fluctuations in a vacuum tube [1]. The noise spectral density is determined by $S_I = 2eI$, where I is the tube's average current. Along with the Johnson–Nyquist noise in thermal equilibrium [2], such fluctuations, now called the shot noise, represent one of the two fundamental sources of current noise in a generic conductor. Careful experiments by Hull and Williams [3] confirmed that the shot noise is observable in the current saturation regime of the vacuum tube and provides a way to measure the elementary charge as accurate as in Millikan's oil-drop experiment. Some 70 years later, shot noise experiments demonstrated $e/3$ quasiparticle charge in the fractional quantum Hall effect (FQHE) [4, 5], one of the milestones in modern physics.

Diluted electron flow in a vacuum tube obeys Poisson statistics for purely classical reasons [6]. By contrast, in solid-state conductors, the shot noise arises from the random partitioning of a degenerate electron stream owing to scattering off disorder or inhomogeneities [2]. This results in much richer possible outcomes of the shot noise measurement and brings valuable information about charge transport mechanism, making noise an attractive experimental tool in mesoscopic physics.

Already in the simplest case of single-mode quantum phase-coherent conductor, the partition noise acquires binomial statistics [7]. Here, the limits are zero noise in the ballistic case (no scattering) and the full Schottky value in the case of negligible transmission probability, $Tr \ll 1$, (tunneling). In between, the spectral density of the current noise is conveniently expressed by the Fano factor $F = S_I/2eI$, which in this case equals [8] $F = 1 - Tr$. In multi-mode conductors, the current fluctuations in different eigenchannels are independent and the overall F is given by averaging over the eigenvalue distribution [2].

In metallic diffusive conductors, the transmission eigenvalue distribution is universal [9], i.e., independent of the shape, length and dimensionless conductance, so is the Fano factor $F = 1/3$ [10]. In fact, this universality is even much stronger and persists in the classical limit, given the energy relaxation is negligible on the time scale of diffusion across the device [11]. That is, perhaps, why in a number of experiments, from normal metals [12] to topological insulators [13] and semiconducting nanowires [14], $F \approx 1/3$ is reported even though the condition of phase-coherence is apparently not fulfilled.

[1] The article is published in the original.

Obviously, current noise measurements are capable to highlight the features of electronic transport hidden in conductance experiments [2]. In the ballistic regime, vanishing of the shot noise demonstrates that scattering is suppressed [8] without performing a bulky length-dependence statistics. In the localized regime, it brings information about the randomness of hopping transport [15, 16], which is otherwise encoded in the temperature dependence of the conductance [17]. In the diffusive regime, various deviations from $F = 1/3$ can arise from inelastic scattering [11, 18, 19] or due to the presence of built-in tunnel barriers and interfaces [20]. A broader application list includes measurements of electron–phonon cooling rates [21], local [14] thermometry and spectroscopy [22], spin-to-charge conversion [23–25], investigation of Coulomb interaction effects [23–25] and proximity induced superconducting correlations [13, 31–34].

This article gives a brief overview of our recent research and is mainly intended to illustrate the strength and, perhaps, the beauty of the noise measurements approach. The body of the paper is divided into five sections, which are largely mutually independent. In Section 2, we investigate the noise in the hopping regime in a quantum Hall (QH) insulator. Section 3 is devoted to the shot noise of the edge transport in HgTe inverted band quantum wells. Section 4 addresses the problem of interface quality in semiconducting nanowires with metallic contacts. In Section 5, we study shot noise in a Coulomb blockaded carbon nanotube. Section 6 gives the estimate of the voltage noise in a resistive state of a superconducting film owing to spontaneous fluctuations of electronic temperature.

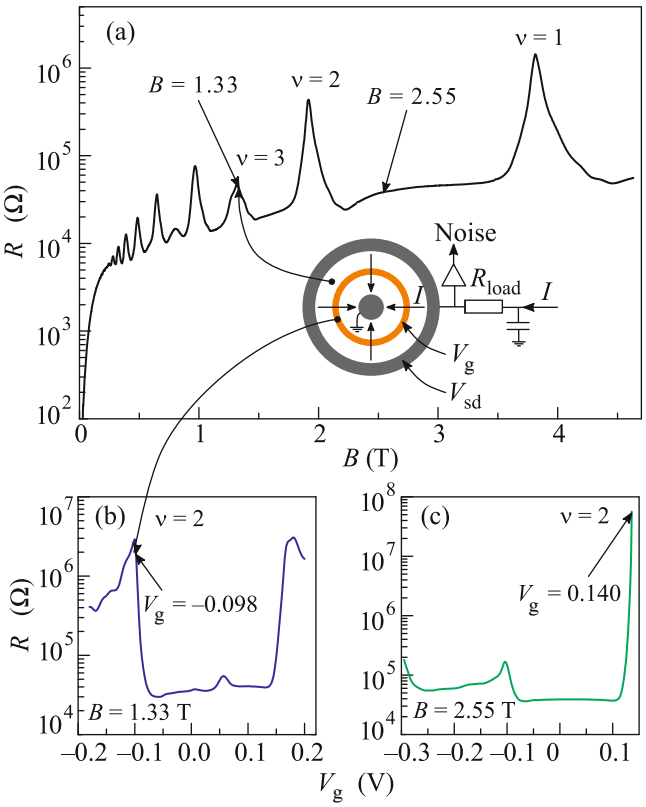

Fig. 1. (Color online) Transport measurements and the parameters choice. (a) Device resistance $R \propto 1/\sigma_{xx}$ as a function of the magnetic field B at zero gate voltage. Inset: device schematics and the measurement configuration. (b, c) Dependence of R on the gate voltage V_g in B = 1.33 T (b) and in B = 2.55 T (c). Arrows mark V_g values used for the noise experiments.

2. SHOT NOISE OF A QUANTUM HALL INSULATOR

In this section, we address the statistics of current flow via insulating states realized in high-quality two-dimensional electron system (2DES) in GaAs in quantizing perpendicular magnetic fields. In the regime of integer quantum Hall effect (QHE) [35], the Fermi level of 2D electrons falls in the band of localized states and the current preferably flows perpendicular to the electric field. Dissipative transport via localized states is conveniently investigated in the Corbino disk geometry, see the inset of Fig. 1a, which allows one to get rid of the dissipationless Hall current contribution, including edge states.

Along with exponentially strong temperature (T) dependence of the conductance, a marked transport property of the QH insulating states is its strongly nonlinear current–voltage (I–V) response, known as the breakdown of the QHE [36]. Although to our best knowledge, there exists no accepted microscopic description of the corresponding I–V characteristics, at least qualitatively one can define two distinct transport regimes. At small enough currents, which we will address below, conduction in the band of localized states occurs via hopping scenario, nearest-neighbor or variable-range, depending on T. By contrast, at very high currents, breakdown scenario is realized, during which some electrons gain enough energy to ionize a number of localized electrons, analogous to impact ionization. In this regime, the differential conductance increases by several orders of magnitude accompanied by huge current noise [37] with effective Fano factor up to $F \sim 10^3$, which is a clear signature of extreme avalanche bunching of electrons.

Here we concentrate on noise at small enough currents when charge transport occurs via individual hopping events within the band of localized states. In few micrometers long devices, the number of hops across the sample can well be a few tens and the noise becomes sensitive to the distribution of their probabilities, or, equivalently, resistances [17]. In the regime of variable range hopping (VRH), this distribution is exponentially wide and both current and noise are

dominated by the most resistive hops, so-called hard-hops [15, 16]. In this case, the Fano factor is inversely proportional to the number of hard-hops, $F \sim 1/N$, and for $N = 1$ can reach $F \sim 1$, as predicted by theory [38] and consistent with experiments. Remarkably, in GaAs 2DES at low T and deep enough in the insulating regime the Poisson noise with $F = 1 \pm 0.1$ was demonstrated [39]. This motivates us to study shot noise in quantizing magnetic fields, where Poisson current statistics would enable, e.g., a direct measurement of the quasiparticle charge in the bulk of the insulating state in the FQHE.

Our device is made of high-quality 2DES of a GaAs/AlGaAs heterostructure with 2D electrons buried 200 nm below the surface. The as-grown electron density and mobility (at 4.2 K) of the 2DES are, respectively, 0.96×10^{11} cm^{-2} and 4×10^6 cm^2/V s. On the surface of the structure, we defined a Corbino disk device, schematically shown in Fig. 1a. The gate electrode encircles the inner Ohmic contact and has the width $L \approx 3$ μm and is 2.15 mm in perimeter. The distance between inner and outer Ohmic contacts is 120 μm. All transport measurements were performed using dc excitation in a ^{3}He insert and the noise setup is calibrated by Johnson–Nyquist thermometry.

Figure 1 illustrates the procedure of the parameter choice for the noise measurements. The B-field is chosen so that the Landau level filling factor in the bulk is somewhat below or above $\nu = 2$. In these cases, see the arrows in Fig. 1a, the Fermi level falls in the band of delocalized states (note still hardly resolved $\nu = 3$ spin gap at $B = 1.33$ T) and the resistance of the device at $V_g = 0$ does not exceed about 50 kΩ. After that, we vary the gate voltage thus tuning the filling factor under the gate close to the integer value $\nu = 2$ (Figs. 1b and 1c). Here, the cyclotron gap opens in the 2DES under the gate and the resistance increases by at least two orders of magnitude, with exponentially strong T dependence.

Figures 2a and 2b show the dependences of shot noise and voltage across the device, respectively, on the current for the chosen combinations of B and V_g. For comparison, the data obtained in the absence of magnetic field in the regime of hopping conduction at $V_g = -0.313$ V are also shown. All the I–V curves in Fig. 2b are strongly nonlinear, which is typical for conduction via localized states [40–42], and become more resistive at increasing B. For instance, the linear response resistance is almost two orders of magnitude higher in $B = 2.55$ T than in $B = 0$. However, the trend in the shot noise is opposite. As is seen in Fig. 2a, at increasing magnetic field the shot noise gradually drops from the Poisson value $F = 1$ in $B = 0$ to $F \sim 0.25$ in $B = 2.55$ T. The finding of shot noise reduction in the insulating states in quantizing magnetic fields is the central result of this section. We briefly discuss it below.

The observation of $F = 1$ in $B = 0$ reproduces our previous result [39] and signals that transport in zero field occurs via VRH conduction in the regime of finite-size effect, when the width of the gate, L, is not greater than the size of the critical cluster, ξ. Compared to longer devices with $L \gg \xi$ in which the random resistance network is very well interconnected [17], see the sketch c1 of Fig. 2c, in the finite-size regime the network splits into a number of quasi-1D hopping chains. They provide independent current paths connected in parallel [43], see the sketch c2 of Fig. 2c. In a magnetic field, naively, one would expect that the finite-size effect further strengthens, for $\xi \propto g^{-7/9}a^{-5/9}$ and both g, the density of states at the Fermi level, and a, the localization radius, are expected to decrease at increasing B. In principle, there are two possibilities to explain the observed reduction of the shot noise by a factor of ~3. The first, and fantastic, possibility would be the reduction of the quasiparticle charge in the 2DES owing to the fractional correlations [4, 5]. This scenario, however, is highly unlikely since FQHE in similar structures is very weak in such small magnetic fields [44] and no signatures of the fractional gaps are seen in Fig. 1a. The second possibility is that the process of thermal activation of electrons towards delocalized states starts to contribute to transport in quantizing magnetic field. This might result from the B-driven suppression of the conductance of VRH network, $\ln G \propto -g^{-1/3}a^{-2/3}T^{-1/3}$. Note, however, that in the QH regime thermally delocalized electrons cannot directly take part in dissipative transport since they drift long distances perpendicular to the electric field [45]. Nevertheless, a variety of choices for the next hop, which emerges in the course of this drift, favors the escape of electrons from the most resistive pathways. In this way, quasi-1D hopping chains interconnect under the gate, see the sketch c3 of Fig. 2c, and hopping becomes less random thereby reducing the shot noise. Our measurements demonstrate that reaching the Poisson current statistics in quantizing magnetic fields is much more challenging compared to the $B = 0$ case. Technically, this makes the possibility of the direct quasiparticle charge measurement in the bulk of a QH insulator extremely difficult.

3. NOISE OF EDGE CHANNELS IN A 2D TOPOLOGICAL INSULATOR

The recently introduced topological insulators are a class of materials with an insulating bulk and conducting helical surface states [46]. The core property of these states is the direct correspondence between electron spin and momentum, called spin-momentum locking, which suppresses elastic disorder scattering by the angle of π. For 2D topological insulators, where the bulk material is a quantum well (QW) [47–49] or a monolayer crystal [50, 51] the surface states represent

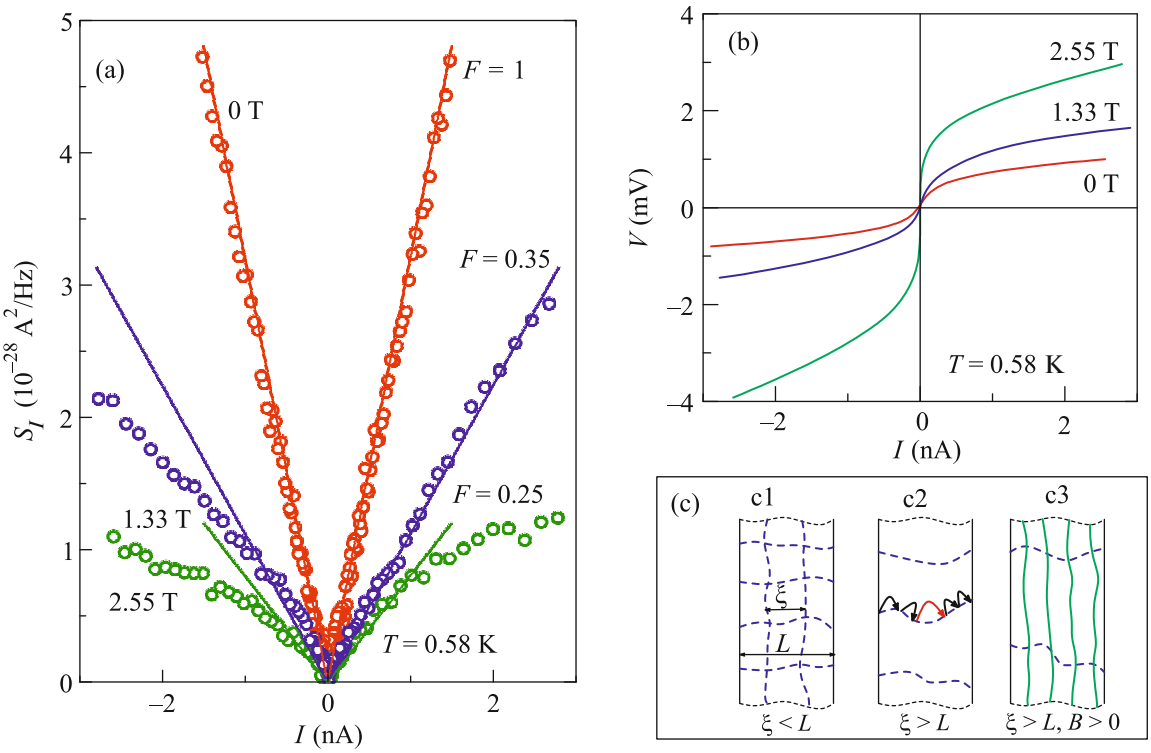

Fig. 2. (Color online) Noise and transport in quantized magnetic fields. (a) Dependence of the noise spectral density S_I on the current I in $B = 1.33$ T at $V_g = -0.098$ V (blue symbols) and in $B = 2.55$ T at $V_g = 0.140$ V (green symbols). For comparison, the data in $B = 0$ at $V_g = -0.313$ V are also shown (red symbols). Solid guides correspond to the fixed Fano factor values of $F = 1$, 0.35, and 0.25. (b) I–V characteristics of the device measured simultaneously with the data in panel (a). Note that the current densities used in our experiment are about two orders of magnitude smaller compared to [37]. (c) Sketches of the current paths in a random resistance network in a long (c1) and short (c2) sample in zero magnetic field and in a short sample in quantizing field (c3).

a 1D single-mode edge conduction channel, known as helical edge states. In this case, the spin-momentum locking strictly prohibits backscattering unless some spin-flip mechanism is present, the property known as topological protection. As a consequence, in the absence of time-reversal symmetry breaking, only inelastic (phase-incoherent) backscattering is allowed, which (i) dictates quantized conductance $G = G_q \equiv e^2/h$ in the limit of $T \to 0$ and (ii) precludes carrier localization, which is inevitable in conventional quasi-1D conductors with a disorder. On the experimental side, the edge transport is clearly demonstrated [52–54] and, in the best devices, a poorly quantized ballistic conductance of $G \approx G_q$ is observed over a few micrometer length scale [48, 54–56]. For longer edges, roughly linear length dependence of the resistance is reported [51, 57] with $G_g/G \propto L$, reminiscent of phase-incoherent diffusive transport. Overall, experiment leaves a certain degree of doubt on the strength of the topological protection, especially in view of the edge transport findings in the trivial phase of InAs/GaSb QWs [58].

Non-equilibrium noise measurements in the regime of edge transport provide additional information about electron scattering and help, at least, to narrow down the list of possibilities. In [59], some of us studied 8 nm wide HgTe QWs in the disordered limit $G \ll G_q$ and measured $0.1 < F < 0.3$. This did not match a well-known [2] phase-coherent 1D single-mode result $F = 1 - Tr \approx 1$, where $Tr \equiv G/G_g$ is the transmission probability. However, in that work, the conclusion about the trivial origin of the edge transport was based on the assumption of dephasing mechanisms not related to spin, which is not the only possibility [60, 105]. The opposite limit was addressed in [22], which considered the shortest possible edges with $G \approx G_q$ realized in lateral p–n junctions of a 14 nm wide HgTe QWs. The observed shot noise is analyzed considering the contact leads overheating. While neither helical edge states nor diffusive multimode scenarios were excluded due to unknown hole-phonon coupling in p-type conduction region, the former scenario was found more consistent.

Here we report measurements of the shot noise in the 14 nm HgTe QWs. Transport measurements in

similar samples were performed in [54] and noise measurements in p–n junctions in [22]. Samples were grown by molecular beam epitaxy, before being shaped in the form of multiterminal hall-bars by wet etching and covered with a 200 nm thick SiO_2/Si_3N_4 insulating layer [61]. On the top of the insulating layer, an Au/Ti metallic gate was deposited, covering the entire hall-bar region. In our devices, the edge lengths varied between 2 and 30 μm, with corresponding conductances in the range $0.3G_q \gtrsim G \gtrsim 0.05G_q$. The measurements were performed in a Bluefors dilution refrigerator at electronic temperatures from 80 mK to 0.8 K, in order to exclude thermally activated bulk conduction (bulk band gap of ≈3 meV reported in [54]). In the present experiment, the contact *1* in Fig. 3a is used to drive current through the two resistive edges *1–2* and *1–3* with lengths 5 and 10 μm, respectively, connected in parallel. We measure both the shot noise and the DC voltage from contact 1.

Figures 3b, 3c are the main results of this section. In the panel (b) the shot noise spectral density is plotted as a function of the device bias current I at different T. At the lowest $T = 80$ mK and $|I| < 5$ nA we observe a clear linear shot noise behavior with a Fano factor $F \approx 0.29$, see the guide line, very close to the universal diffusive value of 1/3. At increasing $|I|$ and/or T the current noise gradually deviates down from the guide-line and the effective Fano factor decreases, e.g., $F \approx 0.09$ at $T = 0.8$ K. At the same time, see Fig. 3c, the linear response resistance, R, exhibits a weakly insulating temperature dependence increasing roughly by 10% at decreasing T from 0.8 K to 80 mK. In the following, we briefly discuss these results in the context of possible transport scenarios.

On the one hand, the observation of shot noise Fano factor very close to the universal value $F = 1/3$ in diffusive conductors [10, 11] evidences diffusive edge transport in our devices, with negligible energy relaxation. On the other hand, that diffusive transport is observed for edge conductances much smaller than G_q, obviously, implies strong dephasing, regardless of the edge transport scenario [9, 62]. In the case of trivial multi-mode edge conduction, slightly insulating T-dependence of the resistance in Fig. 3c can be attributed to a weak localization correction in the limit of dephasing length smaller than localization length. In this case, the correction to the universal value $F = 1/3$ is still expected to be small, yet positive [2]. In the case of helical edge states, our data allow to exclude e–e scattering as a relevant backscattering mechanism in generic helical liquids [63, 64]. In this situation, one would expect metallic T dependence of the resistance and Fano factor [18, 19] $F > 1/3$, which is opposite to our experiment. The microscopic model of random charge-puddles coupled to helical edge states [65] is inconsistent with the $R(T)$ data in Fig. 3c. However, a more general phenomenological model of

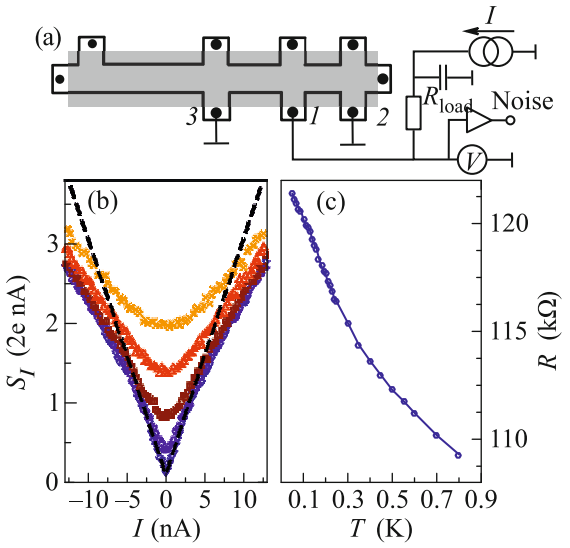

Fig. 3. (Color online) (a) Device schematics and measurement configuration, including load resistance, DC, and noise measurement circuits connected to contact *1*. (b) Shot noise measurements versus bias current. The symbols represent shot noise, measured in configuration (a) at temperatures (top to bottom) 800 mK (crosses), 600 mK (triangles), 400 mK (squares), 200 mK (hexagons), and 80 mK (diamonds). The dashed line is the shot noise prediction with $F = 0.29$ at 80 mK. (c) Two-terminal linear-response resistance of a 5 μm long edge *1–2* as a function of temperature obtained in a different cooldown.

[60] captures our noise data correctly, provided negligible energy relaxation and sufficient spin-flip rate within a puddle. In order to explain the behavior of $R(T)$, however, an increase in the spin-flip rate at decreasing T is necessary, which might be a problem for theory in our temperature range. Scenarios of time-reversal symmetry breaking owing to magnetic impurities [66] or hyperfine interaction [67, 68] predict negative corrections to the conductance without energy relaxation to the bath, which would be qualitatively consistent with our data. Yet, the numerical estimates of these effects in HgTe QWs are unrealistically small [66, 68].

4. NOISE PROBES INTERFACE TRANSPARENCY IN HYBRID STRUCTURES

The theoretical possibility to realize hybrid topological materials [69] has recently led to the revival of experimental interest in inducing superconducting correlations into semiconducting materials. Currently, the most relevant direction is proximitizing quasi-one-dimensional nanowires (NWs) either grown individually [33, 70, 71] or realized in 2D electron gas [72–74]. For all possible applications, the quality of both the one-dimensional conductor and of the semiconductor–superconductor interfaces are of para-

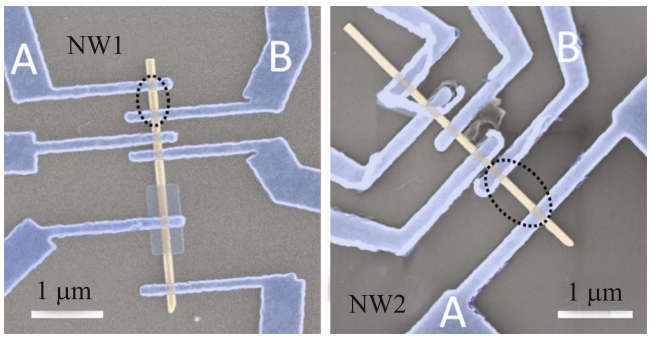

Fig. 4. (Color online) False color SEM images of the studied devices. The NW sections between contacts A and B (dashed ovals) were used for transport and noise measurements.

mount importance. In this section, we demonstrate how noise measurements may complement simple transport measurements in order to better track the possible influence of any present potential barriers.

To illustrate this idea we present experimental data obtained on individually grown semiconductor NWs with Al interfaces. Unintentionally doped catalyst-free InAs NWs were grown by MBE on a Si(111) substrate [75]. The NWs were then detached from the substrate in an ultrasonic bath and drop-casted on a piece of commercial n^+-doped Si wafer covered by 300 nm of SiO_2. In order to remove the native oxide layer from the contact regions, prior to the electron beam evaporation of Al otherwise identical samples NW1 and NW2 were in-situ exposed to Ar ion gun (4.5 sccm Ar flow, 40 V discharge, and 400 V accelerating voltage) during 2 and 4 min, respectively. The latter time is presumably too large and might have led to over-etching of the device NW2 under electrodes and, thus, to bad Al/InAs interfaces. The evaporation was performed in a Plassys MEB 550S system. The measurements were performed in a dry Bluefors dilution refrigerator with the electronic temperature of ≈120 mK, verified by noise thermometry.

False color SEM (scanning electron microscope) images of the studied devices are shown in Fig. 4. The Al contact electrodes are nominally 100 nm wide. We will discuss the data obtained on the NW sections between electrodes A and B, which are 300 and 700 nm long for devices NW1 and NW2, respectively.

In Fig. 5a we plot the bias dependence of the differential conductance, $G = dI/dV$, both in zero, $B = 0$ T (solid lines), and non-zero, $B = 120$ mT (dashed lines), magnetic fields for various back gate voltages V_g. In the shorter device NW1 we observe the supercurrent at $V_g = 30$ V and the large zero-bias conductance peak at $V_g = 0$ V. In Fig. 5a, these features are obtained by numerical differentiation of the I–V-curves, while the larger-bias data are obtained by the

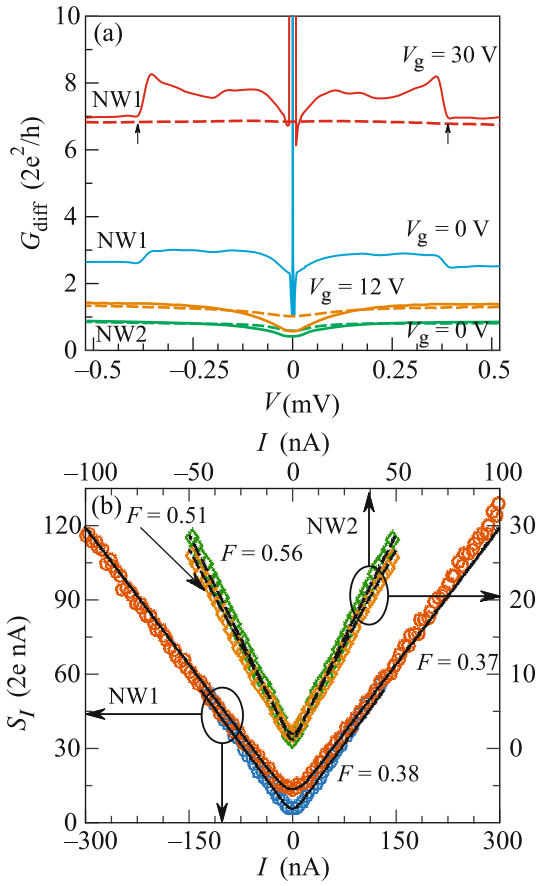

Fig. 5. (Color online) (a) Differential conductance against bias voltage for two devices NW1 and NW2 at various gate voltages. Solid and dashed lines are obtained in $B = 0$ and $B = 120$ mT, respectively. (b) The corresponding noise spectral current density in $B = 120$ mT at electronic temperature $T = 120$ mK. The data for NW1 and NW2 are built, respectively, in left-bottom and right-top axes. The right and the left axes are in the same units.

lock-in measurements with ac current modulation of 1.5 nA rms (root mean square).

The comparison of traces obtained in superconducting and normal states may indicate the better quality of Al/InAs interfaces in the NW1 device compared to the NW2 device. Indeed, in NW1 in $B = 0$ T we observe the increase in G at sub-gap voltages, starting abruptly at approximately twice the superconducting energy gap of Al: $|V| \approx 2\Delta/e \approx 380$ μV, see vertical arrows. Microscopically, this sub-gap enhancement above the normal-state conductance G_N reflects the Andreev reflection charge transport taking place at Al/InAs interfaces and is distinctive for transmissive SNS (Superconductor–Normal–Superconductor) structures [76, 77]. The observation of the supercurrent/large zero-bias conductance $G_S = G$ ($V = 0$, $B = 0$) further suggests the good quality of the interfaces in the device NW1. We note that these features

remain in NW1 at lower gate voltages when the normal-state resistance of the device is about $2e^2/h$. On the contrary, in NW2, in the sub-gap region at bias voltages $|V| \lesssim 100$ μV, we observe the decrease in the conductance below the normal-state value in all the available range of V_g. Such a behavior is inherent in nanostructures of a tunnel type [71] and reflects the fact that Andreev reflection requires two transmission events [78]. The normal-state conductance is thus higher being proportional to the first power of transmission eigenvalues.

Altogether, the data of Fig. 5a display the difference between the devices NW1 and NW2. This difference is additionally manifested in its shot noise in the normal state in magnetic field. In Fig. 5b, we demonstrate the shot noise of the devices NW1 (left-bottom axes) and NW2 (right-top axes, the scales on both axes are enlarged by a factor of 3 and the data are vertically offset by $2e \times 10$ nA for clarity) obtained in $B = 120$ mT at the same values of V_g as in Fig. 5a. For both samples we observe linear $S_I(I)$-dependences characteristic of elastic transport. In NW1, the Fano-factor $F \approx 0.37$ is almost independent of V_g and is only slightly greater than the universal value $F_0 = 1/3$, characteristic for diffusive elastic conduction mechanism. The shot noise in NW2 is significantly greater with $F \gtrsim 0.5$, slightly increasing with increasing resistance in the available gate voltage range. In the following, we discuss the device NW2 since for NW1 we cannot reliably exclude the influence of experimental uncertainty. In principle, the conductance diminishing in the sub-gap region and the accompanying enhanced shot noise in the device NW2 might result from the possibly present tunnel barriers [62]. These might be caused by the short-period wurtzite segments in our polytypic InAs NWs [79] or, alternatively, represent the barriers in the vicinity of Al/InAs interfaces, which result from disorder or band bending due to change in electrostatics after deposition of Al [80].

The Fano-factor of the phase-incoherent diffusive conductor with planar tunnel barriers Γ_i is given by

$$F = F_0\left(1 + 2\frac{\sum_{i=1}^{n} R_{\Gamma_i}^3}{\left(\sum_{i=1}^{n} R_{\Gamma_i} + R_D\right)^3}\right),$$

where R_{Γ_i} is the resistance of the ith barrier, n is the number of barriers, and R_D is the sum of the resistances of diffusive pieces. According to this expression, the experimental observation of $F \gtrsim 0.5$ in NW2 then necessarily requires that the resistance of the device be dominated by the resistance of a single tunnel barrier Γ with $R_\Gamma \gtrsim 2R_D$. Were it the interfacial barrier, we can roughly estimate the ratio of the normal-state and zero-field zero-bias conductances using the result of Nazarov [81]. Numerically, we find $G_N/G_S \approx 1.7$ and 2.1 at $V_g = 12$ and 0 V, respectively, which is in reasonable agreement with the experimentally observed ratios of 1.7 and 1.4. While this may point in favor of the interfacial barrier, we emphasize that our data also do not exclude the structural defect scenario. Concluding this section, we note that the data presented here is, to our best knowledge, the first attempt to verify the role of the built-in tunnel barriers from simultaneous transport and noise measurements in diffusive semiconductor- superconductor hybrid structures.

5. SHOT NOISE IN A CARBON NANOTUBE QUANTUM DOT

The randomness of electronic transport in mesoscopic conductors in many cases can be understood within the framework of non-interacting electrons [2]. At first glance, this may seem surprising since in the absence of interactions electrons must be uncorrelated and obey Poisson statistics, just like in Schottky's vacuum tube. In reality, degenerate electrons in solids are extremely correlated owing to the Pauli exclusion principle [7], which is the ultimate reason for the shot noise vanishing in a ballistic conductor [8]. For the same reason, intrinsic ordering of the incident flux can be directly observed in cross-correlation experiments with electronic beams in the QH edge channels [82]. On top of this, additional correlations can arise thanks to the proximity with a superconductor [2] or due to Coulomb interactions between electrons. In the latter case, which we focus on in this section, such effects are most pronounced in quantum dots (QDs), where Coulomb energy represents the largest energy scale.

The simplest (two-terminal) quantum dot is a conductive island weakly coupled to macroscopic leads via tunnel barriers. Here, we investigate a single-walled carbon nanotube (SWCNT) QD with thermally evaporated Ti/Pd/Au leads with thicknesses of, correspondingly, 0.3/5/60 nm and fabricated via standard e-beam lithography technique. The SWCNTs were grown by aerosol CVD process [83, 84] and dry deposited on a Si/SiO_2 substrate. Unlike in lateral quantum dots formed, e.g., in GaAs, here, tunnel barriers naturally result from the Schottky barrier between the SWCNT and the contact metal. The chemical potential of the dot is tuned by the back gate voltage V_{bg}. The atomic force micrograph of the device is shown in Fig. 6 (inset). Nanotube's height measured before all fabrication steps was approximately 1.3 nm, which to best of our knowledge is an indication of a bundle of SWCNTs, since the minimum diameter of a single nanotube we observed was in the range of 0.6–0.8 nm. On top of the SWCNT (faint line), three metallic contacts are evaporated, dividing it into two

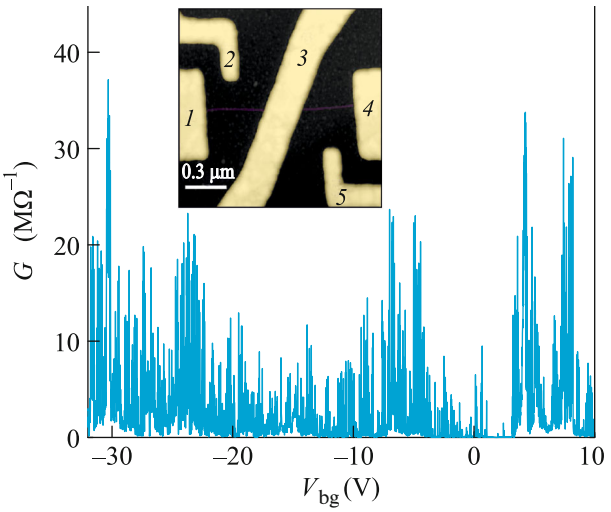

Fig. 6. (Color online) Differential conductance as a function of back-gate voltage at zero applied bias. Inset: atomic force microscopy image (false colors) of the sample. Data discussed in this section were obtained for the left segment of the SWCNT (between metal contacts *1* and *3*).

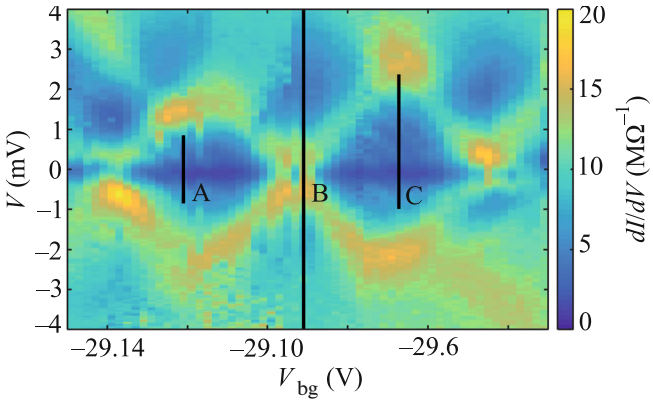

Fig. 7. (Color online) Differential conductance as a function of back-gate voltage V_{bg} and bias voltage V. For three V_{bg} values (marked by solid lines) conductance and noise are represented as a function of bias current I and bias voltage V in Fig. 8 below. Here, the solid lines span only the intervals of V, corresponding to the Fano factor $F \approx 1$ (A, C) and $F \approx 0.5$ (B).

sections, each approximately 400 nm long. Throughout the experiment, the center contact *3* was grounded, the rightmost contact *4* was floating and the dc bias voltage with a small ac modulation was applied to the left contact *1* via the input of a home-made I–V converter (10^7 V/A). The current was measured using standard lock-in technique at 31 Hz modulation frequency. The resonant tank-circuit with the central frequency of 20.9 MHz and a 5 kΩ load resistor was connected to the contact *1* for the shot noise measurements. As usual, the signal was calibrated using Johnson–Nyquist noise thermometry. We used side gates *2* and *5* to check that Coulomb coupling between the two dots on either side of the central contact *3* is negligible; hence, possible charging events on the right QD are irrelevant for the transport and noise measured in the left QD. All the data discussed below are obtained at a bath temperature of 0.5 K in a liquid ^{3}He insert with grounded gates *2* and *5*.

In Fig. 6 (body) we plot V_{bg}-dependence of the linear response conductance of the left SWCNT QD. Within a wide range of V_{bg}, we observe pronounced Coulomb blockade oscillations of irregular amplitude and spacing between neighboring peaks. At slightly positive V_{bg} in the range $1\ \text{V} < V_{bg} < 3\ \text{V}$ the oscillations are suppressed, indicating the energy gap in the spectrum characteristic for semiconducting SWCNTs. Depending on V_{bg} ranges, both oscillations with and without well-developed Coulomb blockade are seen. For some well-developed oscillations (ratio between conductance maxima and minima at least 10) we performed standard finite bias spectroscopy and found the addition energy, which varies between 1 and 5 meV. This scatter is not expected for an individual SWCNT QD, where the fluctuations of single-particle level spacing are typically much smaller than Coulomb energy, determined by the QD capacitance [85, 86]. While it is difficult to draw a definitive conclusion, this might be another indication of a bundle of few SWCNTs connected in parallel. We also cannot exclude an impact of multi-subband transport at large negative V_{bg}. In this case, transport irregularities can be related to a complex interplay of single-particle energy spectrum with intra-SWCNT and inter-SWCNT Coulomb interactions. Below we concentrate on current noise measurements within an arbitrarily chosen pair of adjacent Coulomb blockade resonances and correlate different transport regimes with the current noise measurements.

Figure 7 shows a standard color-scale plot of differential conductance as a function of bias voltage V and V_{bg}. Note that owing to appreciable temporal drifts in our device this data cannot be directly compared to the data of Fig. 6, which were recorded more than a week before. The data of Fig. 7 demonstrates suppressed conductance inside diamond-shaped Coulomb blockade regions. Here, sequential tunneling is forbidden and finite current through the QD occurs only via higher-order co-tunneling processes, which conserve the charge on the QD [87]. Figures 8a–8c, axes on the right-hand side, show three traces of the differential conductance, dI/dV, as a function of V obtained for fixed V_{bg} cuts of the Coulomb diamonds (marked by solid lines in Fig. 7). Traces A and C demonstrate wide conductance minima inside the Coulomb blockade region, followed by conductance maxima at bias voltages roughly corresponding to the boundaries of the

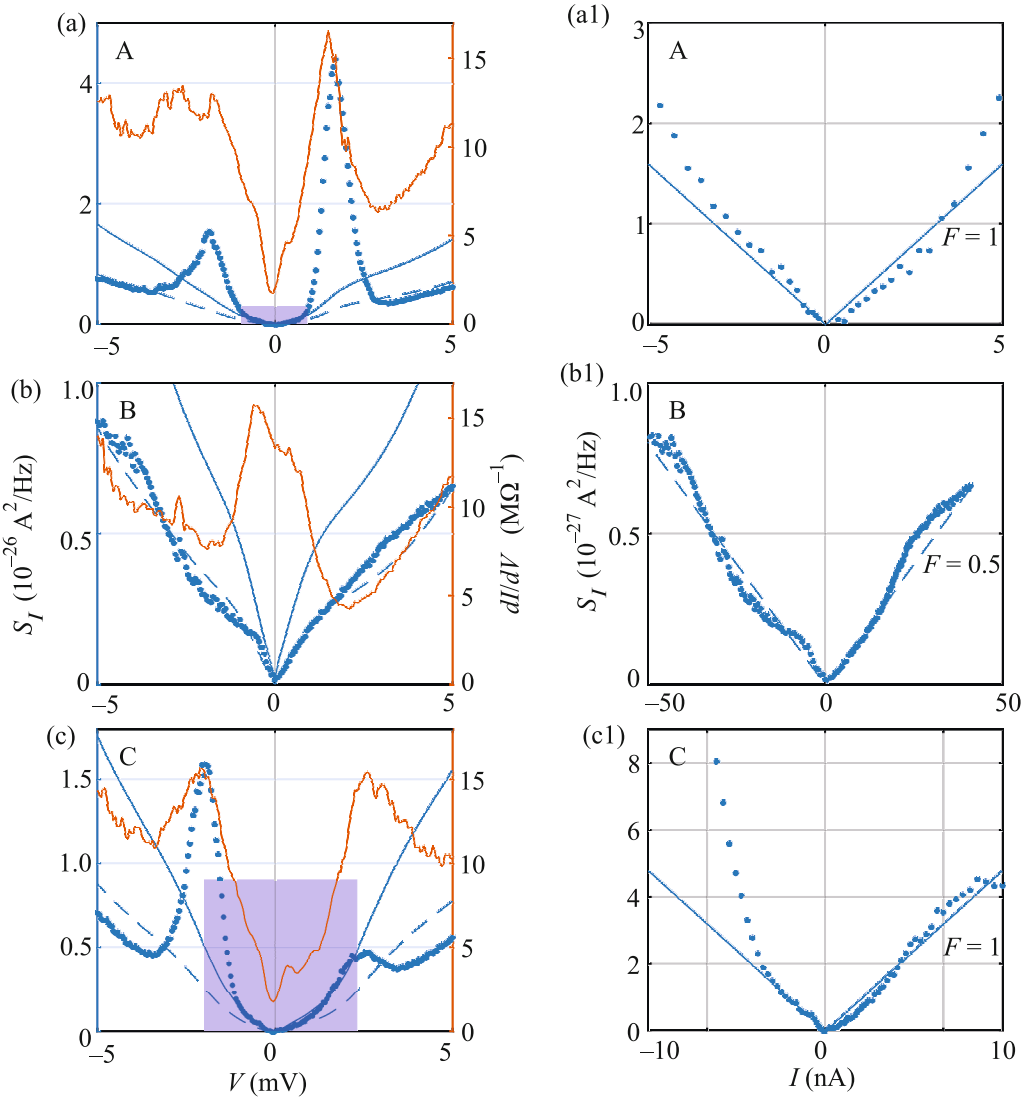

Fig. 8. (Color online) Noise and conductance along three representative cuts. (a)–(c) Current noise spectral density S_I (blue dots, left axis) and differential conductance dI/dV (orange curve, right axis) as a function of bias voltage V for three values of V_{bg} corresponding, respectively, to the cuts A, B, and C in Fig. 7. (a1, b1, c1) S_I as a function of I for the same data as in panels (a)–(c). In panels (a1) and (b1) the data are plotted in the I range, corresponding to shaded regions in panels (a) and (b). Where applicable, blue guidelines indicate the current noise corresponding to the fixed Fano factors $F = 1$ (solid lines) and $F = 0.5$ (dashed lines).

Coulomb diamond structure. As usual, this behavior signals the transition from high order co-tunneling processes at low biases to sequential tunneling at high biases. By contrast, trace B exhibits conductance maximum around $V = 0$, indicating that charge transport near the Coulomb resonance occurs mainly owing to the sequential tunneling via a single quantum level of the SWCNT QD.

The current noise brings more information about microscopic processes underlying SWCNT QD transport. Figures 8a–8c, axes on the left, show the spectral density of current fluctuations measured for the same set of V_{bg}. Depending on the gate voltage position, three distinct types of behavior are observed. First, at small currents and well inside the Coulomb diamonds, see the panels corresponding to traces A and C, the measured noise is close to Poisson value $S_I \approx 2eI$, as shown by solid guidelines. This behavior is expected for the shot noise of elastic co-tunneling process, during which the QD state remains in its ground state [28, 87–89]. Qualitatively, in this case, the electron sees the QD as a single extremely opaque tunnel barrier, just like in a usual non-interacting case [87]. For convenience, the low bias regions highlighted in

Figs. 8a and 8c are represented in the form of $S_I(I)$ plots in Figs. 8a1 and 8c1, respectively. In this representation, the conventional linear shot noise behavior with $F \approx 1$ is evident.

Second, when the QD chemical potential is tuned to the position of Coulomb resonance, see the panels (b) and (b1) of Fig. 8 corresponding to the trace B, the noise is reduced compared to the Poisson value. The reduction is roughly by a factor of 2 and slightly depends on current, see the dashed guideline with $F = 0.5$. The observation of $0.5 \le F \le 1$ is a signature of sequential tunneling in which transport through the QD occurs via two independent tunneling processes across the QD-lead barriers [28, 87–91]. Similar to the non-interacting double-barrier case, this effect is a consequence of current conservation [2, 87] and $F \approx 0.5$ indicates that QD-lead barriers are nearly identical. Close to linear $S_I(I)$ dependence in this case is evident from panel (b1). Passing, we note that at some V_{bg} at small currents we have obtained $0.3 < F < 0.5$, which is difficult to understand in a conventional framework of shot noise in the regime of sequential tunneling. In these situations, however, the SWCNT resistance was typically below 100 kΩ and clear Coulomb diamond structure was not observable.

Third, and perhaps the most striking, is the observation of super-Poisson noise peaks, sometimes with $F \sim 8$, around certain values of V and V_{bg}, see the data for traces A and C near $V \sim \pm 2$ mV. Although much more pronounced, this effect resembles super-Poisson noise maxima observed in random hopping transport via interacting localized states in the insulating phase of *n*-GaAs transistor [16]. In carbon-nanotube QDs the shot noise several times the Poisson value was measured in the regime of inelastic co-tunneling [28, 90]. In general, such a behavior is explained by modulation of the QD current, which occurs owing to the very fast random switching between different quantum states in the regime of Coulomb blockade [87, 88, 92]. Giant noise then is a pure interaction effect not observed, e.g., in SWCNTs in a Fabry–Perot transport regime [91]. In Markovian approximation [87, 93] the modulation noise acquires Lorentzian spectrum and covers the frequency range up to the inverse correlation time of the switching process. Measurements in SWCNTs in the gigahertz regime indicate that the correlation time falls in the range of a few 10 ps [89, 90], which effectively gives rise to super-Poisson white noise at sub-10 GHz frequencies [28], including those used in the present experiment.

As seen from Figs. 8a, 8c, super-Poisson noise maxima correlate with the maxima of differential conductance, which is a clear signature of the modulation noise. Apart from that, however, the low quality of the Coulomb diamonds in our experiment, see Fig. 7, precludes us from unequivocal identification of the microscopic SWCNT QD states participating in the switching process.

6. NOISE AND FLUCTUATIONS OF TEMPERATURE AT A RESISTIVE TRANSITION

Spontaneous fluctuations of current in a conductor at the onset of the transition to the superconducting state (called below the resistive transition) are believed to provide microscopic insight into superconducting correlations. More than 50 years ago, giant low-frequency noise in type-II superconducting films in the magnetic field was associated with the correlated motion of bunches of magnetic vortices [94]. Much smaller noise in disordered type-I films in zero field was interpreted in terms of the motion of independent vortices, emerging from unbinding of vortex-antivortex pairs in a 2D superconductor [95]. Giant noise can also be observed in superconducting weak links [96], originating from fluctuations of the order-parameter [97], multiple [98] or individual quantum [99] phase slips. In the context of transition edge thermometry [100], it was argued that giant noise at the resistive transition can also originate from spontaneous fluctuations of the electronic temperature. Here we present the ab initio estimate of such noise, which is insensitive to the microscopic features of the resistive transition and can dominate the noise spectrum in a wide frequency range.

In thermodynamic equilibrium mean squared fluctuation of the electronic temperature, T_e, is expressed as [101]:

$$\left\langle \Delta T_e^2 \right\rangle = \frac{k_B T_e^2}{C}, \qquad (1)$$

where C is the (electronic) heat capacity and k_B is the Boltzmann constant. We are interested in the spectral density of fluctuations as a function of frequency, $S_T(f)$, which obeys the standard identity $\left\langle \delta T_e^2 \right\rangle = \int S_T(f) df$. Note, that $S_T(f)$ is twice the Fourier transform of the correlation function [93] and can be obtained, e.g., in ac-heating experiments [102]. Typically, such experiments identify Lorentzian-shaped frequency response [103], with characteristic correlation time of a temperature fluctuation, τ, given by the ratio of C and the heat conduction rate to the external bath, G, (both per unit volume), $\tau = C/G$. Below we assume that heat conduction is determined by the electron–phonon (*e–ph*) cooling rate, $G = G_{e-ph}$, and derive from Eq. (1) $S_T(0) = k_B T^2 / G_{e-ph}$, omitting an insignificant for our purposes numerical factor of order unity.

Fluctuations of T_e give rise to fluctuations of the resistance, R, and hence to voltage fluctuations in the

current biased device. These fluctuations are strongest at the resistive transition, where $R(T_e)$ has the strongest temperature dependence. The spectral density of such voltage fluctuations is given by [102] $S_V = I^2 S_R$, where I is the average current and S_R is the spectral density of the resistance fluctuations. Since $S_R = \left(\frac{dR}{dT}\right)^2 S_T$, we obtain:

$$S_V(0) = G_{e-ph}^{-1} I^2 \left(\frac{dR}{dT}\right)^2 k_B T^2, \quad (2)$$

where G_{e-ph} is the total *e–ph* heat conduction of the sample.

In order to estimate the magnitude of voltage fluctuations, we assume that the current biased superconducting film near the sharp resistive transition remains in local thermal equilibrium. In other words, we assume that while Joule heating slightly raises the electronic temperature above the bath, $\delta T_e \equiv T_e - T \ll T$, all the electronic degrees of freedom are mutually equilibrated and the I–V characteristics of the device simply follows the temperature dependence of the resistance $V/I = R(T_e)$. This assumption is reasonable at least in some cases, see [104]. Since δT_e is related to the *e–ph* cooling rate $\delta T_e = (IU) G_{e-ph}^{-1}$, we obtain:

$$S_V(0) = k_B \delta T_e \frac{T^2}{R(T_e)} \left(\frac{dR(T_e)}{dT_e}\right)^2. \quad (3)$$

Under our assumptions, the spectral density of voltage fluctuations is simply determined by the temperature dependence of the resistive transition $R(T_e)$ with T_e as a parameter. Obviously, noise predicted by Eq. (3) can very well exceed the equilibrium Johnson–Nyquist value $S_V/(4k_B TR) \sim T/4\Delta T \gg 1$, provided the width of the resistive transition, ΔT, is small enough. It is also straightforward to see that for high-quality films with R in the range of a few kΩ, our estimate of S_V is much higher than the noises caused by quantum phase slips [99] or by fluctuations of the order-parameter [97]. Unlike these mechanisms, however, the noise owing to thermal fluctuations is insensitive to the microscopic nature of the resistive transition and its spectral density is cutoff at a frequency about the inverse *e–ph* relaxation time [103].

7. CONCLUSIONS

In summary, we discussed several examples how non-equilibrium noise measurements shed light on microscopic aspects of mesoscopic electron transport. Such experiments directly probe electronic correlations, elastic scattering, and energy relaxation in various transport regimes, from normal to superconducting and from ballistic to localized. Hopefully, in this short review, we demonstrated that measuring noise is not only a powerful but also a beautiful approach in experimental condensed matter physics.

We are grateful to Z.D. Kvon, L. Sorba, G. Biasiol, J. Becker, and D. Ruhstorfer for help and to K.E. Nagaev, T.M. Klapwijk, A.V. Semenov, A.G. Semenov, M.A. Skvotsov, G.E. Fedorov, and A.A. Zhukov for stimulating discussions. The experimental work was supported in part by the Russian Science Foundation (project no. 16-42-01050) and theoretical estimation in section 6 was supported by the Russian Science Foundation (project no. 17-72-30036). The work of G.K. was supported by Deutsche Forschungsgemeinschaft (project no. KO-4005/5-1).

REFERENCES

1. W. Schottky, Ann. Phys. **362**, 541 (1918).
2. Y. Blanter and M. Büttiker, Phys. Rep. **336**, 1 (2000).
3. A. W. Hull and N. H. Williams, Phys. Rev. **25**, 147 (1925).
4. R. de Picciotto, M. Reznikov, M. Heiblum, V. Umansky, G. Bunin, and D. Mahalu, Nature (London, U.K.) **389**, 162 (1997).
5. L. Saminadayar, D. C. Glattli, Y. Jin, and B. Etienne, Phys. Rev. Lett. **79**, 2526 (1997).
6. C. Schönenberger, S. Oberholzer, E. Sukhorukov, and H. Grabert, arXiv:0112504 (2001).
7. L. Levitov and G. Lesovik, JETP Lett. **58**, 230 (1993).
8. M. Reznikov, M. Heiblum, H. Shtrikman, and D. Mahalu, Phys. Rev. Lett. **75**, 3340 (1995).
9. C. W. J. Beenakker, Rev. Mod. Phys. **69**, 731 (1997).
10. C. W. J. Beenakker and M. Büttiker, Phys. Rev. B **46**, 1889 (1992).
11. K. E. Nagaev, Phys. Lett. A **169**, 103 (1992).
12. M. Henny, S. Oberholzer, C. Strunk, and C. Schönenberger, Phys. Rev. B **59**, 2871 (1999).
13. E. S. Tikhonov, D. V. Shovkun, M. Snelder, M. P. Stehno, Y. Huang, M. S. Golden, A. A. Golubov, A. Brinkman, and V. S. Khrapai, Phys. Rev. Lett. **117**, 147001 (2016).
14. E. S. Tikhonov, D. V. Shovkun, D. Ercolani, F. Rossella, M. Rocci, L. Sorba, S. Roddaro, and V. S. Khrapai, Sci. Rep. **6**, 30621 (2016).
15. V. V. Kuznetsov, E. E. Mendez, X. Zuo, G. L. Snider, and E. T. Croke, Phys. Rev. Lett. **85**, 397 (2000).
16. S. S. Safonov, A. K. Savchenko, D. A. Bagrets, O. N. Jouravlev, Y. V. Nazarov, E. H. Linfield, and D. A. Ritchie, Phys. Rev. Lett. **91**, 136801 (2003).
17. B. Shklovskii and A. Efros, Springer Ser. Solid-State Sci. **45**, 1 (2013).
18. K. E. Nagaev, Phys. Rev. B **52**, 4740 (1995).
19. V. I. Kozub and A. M. Rudin, Phys. Rev. B **52**, 7853 (1995).
20. Y. V. Nazarov, Phys. Rev. Lett. **73**, 134 (1994).
21. M. L. Roukes, M. R. Freeman, R. S. Germain, R. C. Richardson, and M. B. Ketchen, Phys. Rev. Lett. **55**, 422 (1985).

22. S. Piatrusha and V. Khrapai, in *Proceedings of the 2017 International Conference on Noise and Fluctuations ICNF* (IEEE, 2017).
23. J. Meair, P. Stano, and P. Jacquod, Phys. Rev. B **84**, 073302 (2011).
24. T. Arakawa, J. Shiogai, M. Ciorga, M. Utz, D. Schuh, M. Kohda, J. Nitta, D. Bougeard, D. Weiss, T. Ono, and K. Kobayashi, Phys. Rev. Lett. **114**, 016601 (2015).
25. V. S. Khrapai and K. E. Nagaev, JETP Lett. **105**, 18 (2017).
26. P. Roche, J. Ségala, D. C. Glattli, J. T. Nicholls, M. Pepper, A. C. Graham, K. J. Thomas, M. Y. Simmons, and D. A. Ritchie, Phys. Rev. Lett. **93**, 116602 (2004).
27. Y. Yamauchi, K. Sekiguchi, K. Chida, T. Arakawa, S. Nakamura, K. Kobayashi, T. Ono, T. Fujii, and R. Sakano, Phys. Rev. Lett. **106**, 176601 (2011).
28. M.-C. Harabula, V. Ranjan, R. Haller, G. Fülöp, and C. Schönenberger, Phys. Rev. B **97**, 115403 (2018).
29. H. Inoue, A. Grivnin, N. Ofek, I. Neder, M. Heiblum, V. Umansky, and D. Mahalu, Phys. Rev. Lett. **112**, 166801 (2014).
30. E. S. Tikhonov, M. Y. Melnikov, D. V. Shovkun, L. Sorba, G. Biasiol, and V. S. Khrapai, Phys. Rev. B **90**, 161405 (2014).
31. A. A. Kozhevnikov, R. J. Schoelkopf, and D. E. Prober, Phys. Rev. Lett. **84**, 3398 (2000).
32. B.-R. Choi, A. E. Hansen, T. Kontos, C. Hoffmann, S. Oberholzer, W. Belzig, C. Schönenberger, T. Akazaki, and H. Takayanagi, Phys. Rev. B **72**, 024501 (2005).
33. A. Das, Y. Ronen, M. Heiblum, D. Mahalu, A. V. Kretinin, and H. Shtrikman, Nat. Commun. **3**, 1165 (2012).
34. Y. Ronen, Y. Cohen, J.-H. Kang, A. Haim, M.-T. Rieder, M. Heiblum, D. Mahalu, and H. Shtrikman, Proc. Nat. Acad. Sci. U.S.A. **113**, 1743 (2016).
35. R. Prange, M. Cage, K. Klitzing, S. Girvin, A. Chang, F. Duncan, M. Haldane, R. Laughlin, A. Pruisken, and D. Thouless, *The Quantum Hall Effect, Graduate Texts in Contemporary Physics* (Springer, New York, 2012).
36. G. Eber, K. von Klitzing, K. Ploog, and G. Weinmann, J. Phys. C: Solid State Phys. **16**, 5441 (1983).
37. K. Chida, T. Hata, T. Arakawa, S. Matsuo, Y. Nishihara, T. Tanaka, T. Ono, and K. Kobayashi, Phys. Rev. B **89**, 235318 (2014).
38. Y. A. Kinkhabwala, V. A. Sverdlov, A. N. Korotkov, and K. K. Likharev, J. Phys.: Condens. Matter **18**, 1999 (2006).
39. E. S. Tikhonov, V. S. Khrapai, D. V. Shovkun, and D. Schuh, JETP Lett. **98**, 121 (2013).
40. E. Y. Andrei, G. Deville, D. C. Glattli, F. I. B. Williams, E. Paris, and B. Etienne, Phys. Rev. Lett. **60**, 2765 (1988).
41. H. W. Jiang, R. L. Willett, H. L. Stormer, D. C. Tsui, L. N. Pfeiffer, and K. W. West, Phys. Rev. Lett. **65**, 633 (1990).
42. A. A. Shashkin, V. T. Dolgopolov, G. V. Kravchenko, M. Wendel, R. Schuster, J. P. Kotthaus, R. J. Haug, K. von Klitzing, K. Ploog, H. Nickel, and W. Schlapp, Phys. Rev. Lett. **73**, 3141 (1994).
43. A. S. Rodin and M. M. Fogler, Phys. Rev. B **84**, 125447 (2011).
44. V. S. Khrapai, A. A. Shashkin, M. G. Trokina, V. T. Dolgopolov, V. Pellegrini, F. Beltram, G. Biasiol, and L. Sorba, Phys. Rev. Lett. **100**, 196805 (2008).
45. S. Iordansky, Solid State Commun. **43**, 1 (1982).
46. M. Z. Hasan and C. L. Kane, Rev. Mod. Phys. **82**, 3045 (2010).
47. B. A. Bernevig, T. L. Hughes, and S. C. Zhang, Science (Washington, DC, U. S.) **314**, 1757 (2006).
48. M. Konig, S. Wiedmann, C. Brune, A. Roth, H. Buhmann, L. W. Molenkamp, X. L. Qi, and S. C. Zhang, Science (Washington, DC, U. S.) **318**, 766 (2007).
49. I. Knez, R. R. Du, and G. Sullivan, Phys. Rev. Lett. **107**, 136603 (2011).
50. X. Qian, J. Liu, L. Fu, and J. Li, Science (Washington, DC, U. S.) **346**, 1344 (2014).
51. S. Wu, V. Fatemi, Q. D. Gibson, K. Watanabe, T. Taniguchi, R. J. Cava, and P. Jarillo-Herrero, Science (Washington, DC, U. S.) **359**, 76 (2018).
52. A. Roth, C. Brune, H. Buhmann, L. W. Molenkamp, J. Maciejko, X. L. Qi, and S. C. Zhang, Science (Washington, DC, U. S.) **325**, 294 (2009).
53. K. C. Nowack, E. M. Spanton, M. Baenninger, M. König, J. R. Kirtley, B. Kalisky, C. Ames, P. Leubner, C. Brüne, H. Buhmann, L. W. Molenkamp, D. Goldhaber-Gordon, and K. A. Moler, Nat. Mater. **12**, 787 (2013).
54. E. B. Olshanetsky, Z. D. Kvon, G. M. Gusev, A. D. Levin, O. E. Raichev, N. N. Mikhailov, and S. A. Dvoretsky, Phys. Rev. Lett. **114**, 126802 (2015).
55. K.-M. Dantscher, D. A. Kozlov, M. T. Scherr, S. Gebert, J. Bärenfänger, M. V. Durnev, S. A. Tarasenko, V. V. Bel'kov, N. N. Mikhailov, S. A. Dvoretsky, Z. D. Kvon, J. Ziegler, D. Weiss, and S. D. Ganichev, Phys. Rev. B **95**, 201103 (2017).
56. T. Li, P. Wang, G. Sullivan, X. Lin, and R.-R. Du, Phys. Rev. B **96**, 241406 (2017).
57. G. M. Gusev, Z. D. Kvon, E. B. Olshanetsky, A. D. Levin, Y. Krupko, J. C. Portal, N. N. Mikhailov, and S. A. Dvoretsky, Phys. Rev. B **89**, 125305 (2014).
58. F. Nichele, H. J. Suominen, M. Kjaergaard, C. M. Marcus, E. Sajadi, J. A. Folk, F. Qu, A. J. A. Beukman, F. K. de Vries, J. van Veen, S. Nadj-Perge, L. P. Kouwenhoven, B.-M. Nguyen, A. A. Kiselev, W. Yi, M. Sokolich, M. J. Manfra, E. M. Spanton, and K. A. Moler, New J. Phys. **18**, 083005 (2016).
59. E. S. Tikhonov, D. V. Shovkun, V. S. Khrapai, Z. D. Kvon, N. N. Mikhailov, and S. A. Dvoretsky, JETP Lett. **101**, 708 (2015).
60. P. P. Aseev and K. E. Nagaev, Phys. Rev. B **94**, 045425 (2016).
61. Z. D. Kvon, E. B. Olshanetsky, D. A. Kozlov, E. Novik, N. N. Mikhailov, and S. A. Dvoretsky, Physics **37**, 202 (2011).
62. M. de Jong and C. Beenakker, Phys. A (Amsterdam, Neth.) **230**, 219 (1996).
63. T. L. Schmidt, S. Rachel, F. von Oppen, and L. I. Glazman, Phys. Rev. Lett. **108**, 156402 (2012).
64. N. Kainaris, I. V. Gornyi, S. T. Carr, and A. D. Mirlin, Phys. Rev. B **90**, 075118 (2014).

65. J. I. Väyrynen, M. Goldstein, and L. I. Glazman, Phys. Rev. Lett. **110**, 216402 (2013).
66. P. D. Kurilovich, V. D. Kurilovich, I. S. Burmistrov, and M. Goldstein, JETP Lett. **106**, 593 (2017).
67. C. H. Hsu, P. Stano, J. Klinovaja, and D. Loss, Phys. Rev. B **96**, 1 (2017).
68. C.-H. Hsu, P. Stano, J. Klinovaja, and D. Loss, Phys. Rev. B **97**, 125432 (2018).
69. J. Alicea, Rep. Prog. Phys. **75**, 076501 (2012).
70. V. Mourik, K. Zuo, S. M. Frolov, S. R. Plissard, E. P. A. M. Bakkers, and L. P. Kouwenhoven, Science (Washington, DC, U. S.) **336**, 1003 (2012).
71. H. O. H. Churchill, V. Fatemi, K. Grove-Rasmussen, M. T. Deng, P. Caroff, H. Q. Xu, and C. M. Marcus, Phys. Rev. B **87**, 241401 (2013).
72. J. Shabani, M. Kjaergaard, H. J. Suominen, Y. Kim, F. Nichele, K. Pakrouski, T. Stankevic, R. M. Lutchyn, P. Krogstrup, R. Feidenhans'l, S. Kraemer, C. Nayak, M. Troyer, C. M. Marcus, and C. J. Palmstrom, Phys. Rev. B **93**, 155402 (2016).
73. M. Kjaergaard, H. J. Suominen, M. P. Nowak, A. R. Akhmerov, J. Shabani, C. J. Palmstrom, F. Nichele, and C. M. Marcus, Phys. Rev. Appl. **7**, 034029 (2017).
74. H. J. Suominen, M. Kjaergaard, A. R. Hamilton, J. Shabani, C. J. Palmstrom, C. M. Marcus, and F. Nichele, Phys. Rev. Lett. **119**, 176805 (2017).
75. G. Koblmller, S. Hertenberger, K. Vizbaras, M. Bichler, F. Bao, J.-P. Zhang, and G. Abstreiter, Nanotechnology **21**, 365602 (2010).
76. S. Abay, D. Persson, H. Nilsson, F. Wu, H. Q. Xu, M. Fogelström, V. Shumeiko, and P. Delsing, Phys. Rev. B **89**, 214508 (2014).
77. A. V. Bubis, A. O. Denisov, S. U. Piatrusha, I. E. Batov, V. S. Khrapai, J. Becker, J. Treu, D. Ruhstorfer, and G. Koblmüller, Semicond. Sci. Technol. **32**, 094007 (2017).
78. A. Shelankov, JETP Lett. **32**, 111 (1980).
79. J. Becker, S. Morkötter, J. Treu, M. Sonner, M. Speckbacher, M. Döblinger, G. Abstreiter, J. J. Finley, and G. Koblmüller, Phys. Rev. B **97**, 115306 (2018).
80. M. T. Deng, S. Vaitiekenas, E. B. Hansen, J. Danon, M. Leijnse, K. Flensberg, J. Nygård, P. Krogstrup, and C. M. Marcus, Science (Washington, DC, U. S.) **354**, 1557 (2016).
81. Y. V. Nazarov, Phys. Rev. Lett. **73**, 1420 (1994).
82. M. Henny, Science (Washington, DC, U. S.) **284**, 296 (1999).
83. A. Moisala, A. G. Nasibulin, D. P. Brown, H. Jiang, L. Khriachtchev, and E. I. Kauppinen, Chem. Eng. Sci. **61**, 4393 (2006).
84. Y. Tian, M. Y. Timmermans, M. Partanen, A. G. Nasibulin, H. Jiang, Z. Zhu, and E. I. Kauppinen, Carbon **49**, 4636 (2011).
85. M. Bockrath, Science (Washington, DC, U. S.) **275**, 1922 (1997).
86. S. J. Tans, M. H. Devoret, H. Dai, A. Thess, R. E. Smalley, L. J. Geerligs, and C. Dekker, Nature (London, U.K.) **386**, 474 (1997).
87. E. V. Sukhorukov, G. Burkard, and D. Loss, Phys. Rev. B **63**, 125315 (2001).
88. W. Belzig, Phys. Rev. B **71**, 161301 (2005).
89. J. Basset, A. Y. Kasumov, C. P. Moca, G. Zaránd, P. Simon, H. Bouchiat, and R. Deblock, Phys. Rev. Lett. **108**, 046802 (2012).
90. E. Onac, F. Balestro, B. Trauzettel, C. F. J. Lodewijk, and L. P. Kouwenhoven, Phys. Rev. Lett. **96**, 026803 (2006).
91. F. Wu, P. Queipo, A. Nasibulin, T. Tsuneta, T. H. Wang, E. Kauppinen, and P. J. Hakonen, Phys. Rev. Lett. **99**, 156803 (2007),
92. K. Kaasbjerg and W. Belzig, Phys. Rev. B **91**, 235413 (2015).
93. S. Kogan, *Electronic Noise and Fluctuations in Solids* (Cambridge Univ. Press, Cambridge, 2008).
94. D. V. Ooijen and G. V. Gurp, Phys. Lett. **17**, 230 (1965).
95. R. F. Voss, C. M. Knoedler, and P. M. Horn, Phys. Rev. Lett. **45**, 1523 (1980).
96. T. Hoss, C. Strunk, T. Nussbaumer, R. Huber, U. Staufer, and C. Schönenberger, Phys. Rev. B **62**, 4079 (2000).
97. D. Bagrets and A. Levchenko, Phys. Rev. B **90**, 180505 (2014).
98. M. Žonda, W. Belzig, and T. Novotný, Phys. Rev. B **91**, 134305 (2015).
99. A. G. Semenov and A. D. Zaikin, Phys. Rev. B **94**, 014512 (2016).
100. H. F. C. Hoevers, A. C. Bento, M. P. Bruijn, L. Gottardi, M. A. N. Korevaar, W. A. Mels, and P. A. J. de Korte, Appl. Phys. Lett. **77**, 4422 (2000).
101. L. Landau and E. Lifshitz, *Course of Theoretical Physics,* Vol. 5: *Statistical Physics,* 3rd ed. (Elsevier Science, Amsterdam, 2013; Nauka, Moscow, 1995), eng. p. 340.
102. S. Kogan, Sov. Phys. Usp. **28**, 170 (1985).
103. A. Kardakova, A. Shishkin, A. Semenov, G. N. Goltsman, S. Ryabchun, T. M. Klapwijk, J. Bousquet, D. Eon, B. Sacépé, T. Klein, and E. Bustarret, Phys. Rev. B **93**, 064506 (2016).
104. S. V. Postolova, A. Y. Mironov, and T. I. Baturina, JETP Lett. **100**, 635 (2015).
105. A. Mani and C. Benjamin, Sci. Rep. **7**, 6954 (2017).